Translational Oncology 45 (2024) 101981

Contents lists available at ScienceDirect

Translational Oncology

journal homepage: www.elsevier.com/locate/tranon

Original Research

# A novel SLC3A2-targeting antibody-drug conjugate exerts potent antitumor efficacy in head and neck squamous cell cancer

Meijun Zheng [a,1], Zeng Wang [b,1], Mengyao Li [b], Nian Yang [b], Huaqing Lu [b], Zongliang Zhang [b], Yijun Dong [a], Yongdong Chen [b], Zhixiong Zhu [b], Aiping Tong [b,*], Hui Yang [a,*]

[a] Department of Otolaryngology, Head and Neck Surgery, West China Hospital, West China Medical School, Sichuan University, Chengdu, Sichuan Province, PR China
[b] State Key Laboratory of Biotherapy, West China Hospital, West China Medical School, Sichuan University, Chengdu, Sichuan Province, PR China

ARTICLE INFO

*Keywords:*
Head and neck squamous cell cancer
SLC3A2
Antibody-drug conjugates
ADC

ABSTRACT

The development of innovative therapeutic strategies for head and neck squamous cell carcinoma (HNSCC) is a critical medical requirement. Antibody-drug conjugates (ADC) targeting tumor-specific surface antigens have demonstrated clinical effectiveness in treating hematologic and solid malignancies. Our investigation revealed high expression levels of SLC3A2 in HNSCC tissue and cell lines. This study aimed to develop a novel anti-SLC3A2 ADC and assess its antitumor effects on HNSCC both *in vitro* and *in vivo*. This study developed a potent anti-SLC3A2 ADC (19G4-MMAE) and systematically investigated its drug delivery potential and antitumor efficacy in preclinical models. This study revealed that 19G4-MMAE exhibited specific binding to SLC3A2 and effectively targeted lysosomes. Moreover, 19G4-MMAE induced a significant accumulation of reactive oxygen species (ROS) and apoptosis in SLC3A2-positive HNSCC cells. The compound demonstrated potent antitumor effects derived from MMAE against SLC3A2-expressing HNSCC in preclinical models, displaying a favorable safety profile. These findings suggest that targeting SLC3A2 with an anti-SLC3A2 ADC could be a promising therapeutic approach for treating HNSCC patients.

## Introduction

Head and neck squamous cell carcinoma (HNSCC) is the sixth most prevalent type of cancer globally, with over 830,000 individuals diagnosed and mortality rates ranging from 40% to 50% [1,2]. HNSCC accounts for 90% of all head and neck cancers and encompasses a diverse range of tumors originating from squamous epithelium at various anatomical sites. Major risk factors associated with HNSCC include tobacco use, alcohol consumption, and human papillomavirus infection [3,4]. Standard treatment options for HNSCC include surgery, chemotherapy, radiotherapy, and chemoradiotherapy. Importantly, efficient multidisciplinary team management is pivotal in enhancing HNSCC patients' clinical outcomes and quality of life [5,6]. Despite significant advancements in managing advanced or recurrent head and neck cancers, the 5-year survival rate remains suboptimal [7]. Given these challenges, extensive research efforts are underway to investigate promising novel therapies for HNSCC.

Similar to various other cancer types, HNSCC develops in the context of immune suppression. The dysregulated immune system, particularly in cancer immunosurveillance, promotes the development and progression of head and neck tumors. Consequently, immunotherapy has emerged as a promising approach to managing patients with locally advanced HNSCC[8]. A therapeutic approach that has shown clinical efficacy in HNSCC is the use of antibody-drug conjugates (ADC). These ADCs employ a chemical linker to attach cytotoxic payloads to a monoclonal antibody, aiming to enhance delivery to target cells while minimizing exposure to normal cells [9]. ADC undergoes internalization through antigen-mediated endocytosis after binding to the surface of target tumor cells. Subsequently, the protein component is degraded in lysosomes, releasing cytotoxic payloads, ultimately triggering cell apoptosis and death [10]. Various payloads, including paclitaxel [11], vinblastine [12], and epothilone [13], have been effectively utilized in clinical settings. While some ADCs have demonstrated responses, their overall efficacy falls short compared to immunotherapies used in

*Abbreviations:* HNSCC, head and neck squamous cell cancer; ADCs, solute carrier family 3 member 2, SLC3A2; lysosomes associated membrane protein 1, LAMP1, antibody-drug conjugates; ROS, reactive oxygen species; DAR, drug to antibody ratio.

* Corresponding authors at: No. 37 Guo Xue Xiang Chengdu, 610041 PR China.
*E-mail addresses:* aipingtong@scu.edu.cn (A. Tong), yh8806@163.com (H. Yang).

[1] These authors contributed equally to the manuscript.

https://doi.org/10.1016/j.tranon.2024.101981
Received 22 February 2024; Received in revised form 3 April 2024; Accepted 27 April 2024

hematological malignancies, partly due to the diverse antigen expression in solid tumors. Thus, the development of more targeted therapeutic agents is essential for enhancing the antitumor effectiveness and expanding treatment options in HNSCC.

Solute carrier family 3 member 2 (SLC3A2) is the most typical member of the SLC family, encoding the heavy chain of CD98 (CD98hc) [14]. Together with the LAT1 (SLC7A5), the LAT1/CD98hc complex facilitates the uptake of various amino acids such as isoleucine, leucine, methionine, valine, histidine, tyrosine, and tryptophan. SLC3A2 shows high expression levels in numerous malignant tumors, including myeloma [15], renal cancer [16], lung cancer [17], breast cancer [18] and head and neck squamous cell cancer [19], lymphoma [20] and leukemia [21]. Its expression has been associated with the progression and metastasis of several human carcinomas [22]. Importantly, Milkereit et al. demonstrated that LAPTM4b can recruit LAT1-CD98hc to lysosome [23], suggesting that SLC3A2 efficiently internalizes molecules to reach the lysosomal compartment, enabling the delivery of potent payloads to the cytosol and enhancing the efficacy of ADC therapeutics. The SLC7A5/SLC3A2 interaction also involves processes such as ferroptosis, apoptosis, and autophagy-driven cell death [24,25]. These characteristics position SLC3A2 as a promising candidate for developing ADCs, making it a viable target for therapeutic intervention in HNSCC.

This study developed a novel SLC3A2-targeting ADC, 19G4-MMAE, which combines a humanized chemic SLC3A2 monoclonal IgG1 antibody (19G4) as the targeting component with a potent cytotoxic drug MMAE as the payload component. The objective was to assess the efficacy of the SLC3A2-targeted MMAE ADC in HNSCC cell lines and tumor models. Both *in vitro* and *in vivo* experiments revealed a significant and selective anti-tumor activity of the anti-SLC3A2 ADC against human HNSCC cell lines and tumors. The findings suggest that this innovative conjugate holds promise as a treatment option for SLC3A2-positive HNSCC.

## Materials and methods

### *Cell lines and cell culture*

Human HNSCC cell lines FADU, SCC15, NPC/HK1, C666-1, SNU-46, SNU-899 were purchased from ATCC. FADU, SNU-46 and SNU-899 were cultured in DMEM (Gibco) containing 10% fetal bovine serum and 1.0 mmol/L penicillin-streptomycin combination (Hyclone). SCC15, NPC/HK1, and C666–1 were cultured in 1640 medium added in 10% fetal bovine serum. All cell lines were incubated in a humidified atmosphere at 37 °C containing 5% $CO_2$.

### *Preparation of 19G4-MMAE, IGG-MMAE*

Specific monoclonal antibody against SLC3A2 (clone 19G4) was generated by our group using a standard hybridoma technique. The anti-SLC3A2 monoclonal antibody, clone 19G4 and isotype control IgG (human IgG; Bioss, Beijing, China) were used to construct ADC. 19G4 or control IgG was diluted to a final concentration of 10 mg/mL. 10-fold molar equivalents of tris(2-carboxyethyl) phosphine (TCEP) were added to the antibody to liberate the thiol residues. The reaction mixture was incubated at 37 °C for 3 h. The partially reduced 19G4 or control IgG was diluted to 10 mg/mL with 20 mM Na2HPO4/NaH2PO4, 20 mM NaCl, 1 mM EDTA pH 7.0 before conjugation with mc-PAB-MMAE. 10 mM mc-PAB-MMAE. In DMSO was added to 5-fold molar equivalents and the conjugation reaction was proceed for 3 h at 25 °C fold. The crude ADC was buffer exchanged into 20 mM Na2HPO4/NaH2PO4, 50 mM NaCl, pH 7.0 to remove unconjugated payloads.The drug-antibody ratio (DAR) of 19G4-MMAE was confirmed by LC-MS (Chengdu SciMount Pharmatech Co., Ltd) .

### *Flow cytometry assays*

Cell surface expression level of SLC3A2 were analyzed by flow cytometry. Briefly, cells (FADU, SCC15, NPC/HK1, SNU-46, SNU-899, C666–1) were collected by centrifugation and incubated with antibodies specific to human SLC3A2 (BioLegend, San Diego, CA, USA) for 30 min in the dark on ice. After washing twice with ice-cold flow cytometry buffer, the cells were resuspended in 300 μL flow cytometry buffer and analyzed the cells using FACS Fortessa (BD Biosciences). The binding affinity of 19G4 to SLC3A2 positive HNSCC cell lines was also determined by flow cytometry assay. $2 \times 10^5$ cells were incubated with 19G4-MMAE in PBS for 30 min on ice. Then cells were washed twice with PBS and incubated with FITC–conjugated Affinipure Goat Anti-human IgG(H+L) at 1:400 for 30 min on ice. After twice of wash, cells were analyzed using FACS Fortessa (BD Biosciences). Each sample were analyzed via FlowJo-V10 software(v.10.6.0; https://www.flowjo.com).

### *Internalization of 19G4-MMAE*

To examined the inernalization of cell surface-bound 19G4-MMAE, cells were incubated with 19G4-MMAE (10 μg/mL) in culture medium at 4 °C for 30 min. After twice of wash, cells were incubated at 37 °C for 1 or 6 h to drive internalization. After washing twice with ice-cold PBS, the cells were incubated with FITC–conjugated Affinipure Goat Anti-human IgG(H+L) at 1:400 for 30 min on ice. After washing twice, cells were analyzed by flow cytometry. The internalization of 19G4-MMAE at each time point was determined by MFI:% internalized = (total surface bound (4 °C) − total surface bound (37 °C))/total surface bound (4 °C) × 100%.

### *Confocal microscopy*

FADU, SCC15, NPC/HK1 cells were seeded on glass coverslips in 24-well plates ($1 \times 10^5$ cells per well) and cultured at 37 °C with 5% of $CO^2$ for 24 h. Cells were stained with the SLC3A2 primary antibody (Cell Signaling Technology, CST, Danvers, MA, USA; D3F9D) for 60 min or 12 h at 4 °C then stained with a 594-conjugated secondary antobody (Proteintech, Rosemont, IL, USA) and DAPI (Beyotime Institute of Biotechnology, Shanghai, P. R. China). Thereafter, cells were washed, fixed, and observed using confocal microscopy. For visualized internalization assay by confocal microscopy, cells were seeded at a $3 \times 10^4$ cells/mL were treated with 10 μg/mL of 19G4-MMAE on ice. After washing with PBS, cells were incubated at 37 °C for 0 or 6 h. 19G4-MMAE was detected with FITC–conjugated Affinipure Goat Anti-human IgG(H+L), lysosomes with rabbit monoclonal antibody against LAMP-1 (Sino Biological, Beijing, China, 11,215-R107) followed by Cy3-labeled goat anti-rabbit IgG (H+L) antibody. LC3 immunofluorescence staining was accomplished as describe above, antibody were specific for LC3 (Proteintech, Rosemont, IL, USA, 14600-1-AP).The images were captured using confocal microscopy.

### *Western blotting*

Briefly, Cells treated with different antibodies were collected and lysed in RIPA buffer (beyotime), containing protease inhibitor cocktail (Abcam), and incubated on ice for 1 h with an interval vortex. The lysates underwent centrifugation at 12,000 rpm for 15 min at 4 °C. The total protein concentrations in the resulting supernatant fractions were determined using a BCA protein assay kit (beyotime). Then the equal amounts of protein samples were boiled for 10 min and separated in a 10% SDS-PAGE gel and transferred to nitrocellulose filter membranes. After blocking with 5% milk, the membranes were blotted with LC3 polyclonal antibody (Proteintech), Rabbit PAb (1:2000) and GAPDH antibody (Servicebio), Rabbit PAb (1:3000) incubated in blocking solution overnight at 4 °C, followed by incubation with horseradish peroxidase (HRP)-conjugated goat anti-rabbit secondary antibody

(1:3000) (Proteintech) and visualization with Chemiluminescent Reagent (Bio-Rad, USA).

*Apoptosis assay*

Cells were seeded in 24-well plates at a density of 2.5 × $10^5$ cells/well and exposed to 19G4-MMAE at various concentrations for 48 h. The control group was incubated with medium alone. Then cells were collected and stained with AnnexinV-FITC and 7AAD for apoptosis analysis. The percentages of apoptotic cells (AnnexinV+/PI− and/AnnexinV+/ PI+) were determined by flow cytometric analysis.

*Reactive oxygen species (ROS) detection*

The ROS detection assay was measured using 2′,7′-dichlorofluorescin diacetate (DCFDA) method by ROS assay kit (Beyotime). Briefly, cells were incubated with 10 μM DCFDA in the dark for 1 hour at 37 °C. Then, cells were exposed with different agent treatments at 37 °C for 10 h. After washing, cells were added to glass slides, fluorescence signal intensities indicating ROS levels were examined by flurorescence microscopy.

*In vitro cytotoxicity assays*

The MTT assay was performed to determin the *in vitro* efficacy of the 19G4-MMAE ADC. Cells were seeded in 96-well plates at a density of 5000 cells/well for SCC15, NPC/HK1, FADU, C666–1 at 37 °C and 5% $CO_2$ overnight. Dilutions of PBS, 19G4, IgG-MMAE, and 19G4-MMAE solutions were added to cells for 72 h incubation at 37 °C. Cell viability were evaluated in triplicate by MTT assay. The $IC_{50}$ was determined using Graphpad Prism version 9 (GraphPad Software, Inc.).

*Efficacy of 19G4-MMAE in mouse xenograft tumor models*

Experiments using Balb/c nude female mice were performed in accordance with the Institutional Animal Care and use committee approved protocols. Six to eight weeks old female BALB/c nude mice (GemPharmtech, Jiangsu, China) were inoculated subcutaneously with 5 × $10^6$ SCC15 cells in 100 μL of PBS on the right flank.When tumor volumes reached approximately 150 $mm^3$, mice were randomized into four treatment groups ($n = 5$). The different treatment groups included vehicle PBS, 19G4, IgG-MMAE, and 19G4-MMAE (5 mg/Kg), repesctively. Mice were administered three doses of treatment every 3 days intravenously. Tumor volume [(length × $width^2$)/2] was measured using calipers every 3–4 days. Mice were weighted to evaluate the toxicity of treatment. Animals were euthanized when tumor volumes reached 2000 $mm^3$.

*Immunohistochemistry*

Tumor tissue were analyzed for SLC3A2 expression. All samples were fixed in 10% formalin and embedded in paraffin wax for staining with commercial anti-SLC3A2-rabbit mAb (CST; 1:400). In brief, tumor tissue sections were incubated at 65 °C for 2 h and then were deparaffinized in xylene and rehydrated with decreasing grades of ehanol. After blocking with PBS containing 10% normal goat serum (Boster, Wuhan, P. R. China) for 1 h at room temperature, followed by incubation with anti-SLC3A2 antibody 1:200 at 4 °C overnight. Following atwice of wash, bound primary antibodies were incubated with goat anti-rabbit secondary antibodies, followed by DAB detection (ZSGB-BIO, Beijing, P. R. China).

*Statistical analysis*

All statistical analyses were performed using GraphPad Prism 9.0 software (http://www.graphpad.com). Data are presented as the mean ± standard deviation (SD), Student's *t*-test was performed to compare statistical significance between two groups, $p$ value < 0.05 were considered to be statistically significant.

## Results

*SLC3A2 is highly expressed on the surface in tissues and cell lines of HNSCC*

The mRNA expression levels of SLC3A2 in various cancer types were analyzed using The Cancer Genome Atlas database (TCGA; http://cancergenome.nih.gov). The results showed that SLC3A2 was expressed in multiple cancer types, including HNSCC (Fig. 1**A**). Moreover, higher expression of SLC3A2 was associated with poorer overall survival rates in HNSCC patients, with a statistically significant correlation ($p = 0.024$) (Fig. 1**B**). To determine the prevalence of SLC3A2 expression, HNSCC tissue samples were subjected to IHC staining, revealing positive SLC3A2 staining in 88% (44 out of 50) of HNSCC cancer samples. Among these samples, 76% (38 out of 50) exhibited moderate to strong expression of SLC3A2, scored as 2+ or 3+. In contrast, weak or absent staining of SLC3A2 was detected in normal adjacent HNSCC tissue (Fig. 1**C**). Additionally, the surface expression of SLC3A2 protein in a human HNSCC cell line was assessed using flow cytometry. The results indicated varied levels of SLC3A2 expression in five out of six tested HNSCC cell lines, except for the C666–1 cell line which showed minimal or no SLC3A2 expression (Fig. 1**D**). The cell surface expression of SLC3A2 protein was further validated through immunofluorescence staining in SCC15, NPC/HK1, and FADU cells (Fig. 1**E**), demonstrating membranous localization of SLC3A2. (Fig. 1**C,** 1**E**) The IHC and immunofluorescence staining findings suggest that targeting SLC3A2 could be a promising strategy for HNSCC patient management.

*Generation and characterization of the anti-SLC3A2 ADC*

An anti-SLC3A2 monoclonal antibody (19G4) was produced from female Balb/c mice immunized with the human SLC3A2-ECD-his protein using the traditional hybridoma technique. The affinity ability of the candidate antibodies to SLC3A2 was measured using the Octet R8 (Sartorius) instrument. Based on the affinity of these antibodies, we selected one mAb with higher affinity, clone 19G4, for further research. We conjugate a MMAE to a SLC3A2-targeting monoclonal antibody (19G4), f resulting in 19G4-MMAE (Fig. 2**A**), which showed a similar affinity to SLC3A2 as the 19G4 mAb (KD=2.096 × 10–9 mol·$L^{-1}$ vs. KD=1.693 × 10–9 mol·$L^{-1}$) (Fig. 2**B**). The conjugates exhibited an average (drug to antibody ratio) of 1.63, as detailed in the methods section (Fig. 2**C, Table.S1**). The identities of the 19G4-MMAE were validated through SDS-PAGE analysis (Fig. 2**D**). When subjected to non-reducing conditions, 19G4-MMAE displayed multiple bands representing the distribution of drug-linked species. Reduction of intermolecular chain disulfide bonds released free sulfhydryl groups, enabling the linkers to bind to specific residues and create conjugated mixtures. The binding of 19G4-MMAE to the extracellular domain and SLC3A2-positive cell lines was further assessed through ELISA (Fig. 2**D**) and FCM analysis (Fig. 2**E**), revealing that the binding efficacy of 19G4-MMAE was comparable to that of 19G4 mAb. These findings demonstrated the retention of a high affinity of 19G4-MMAE to SLC3A2, with no significant impact from the MMAE conjugation.

*Internalization of the 19G4-MMAE*

Importantly, efficient antigen-mediated internalization of ADC by target cells is crucial for delivering cytotoxic payload (MMAE) into cancer cells. We conducted an immunofluorescence assay to confirm the internalization and lysosomal targeting of 19G4-MMAE. NPC/HK1 and SCC15 cells were exposed to 19G4-MMAE and incubated at 37 °C for 1

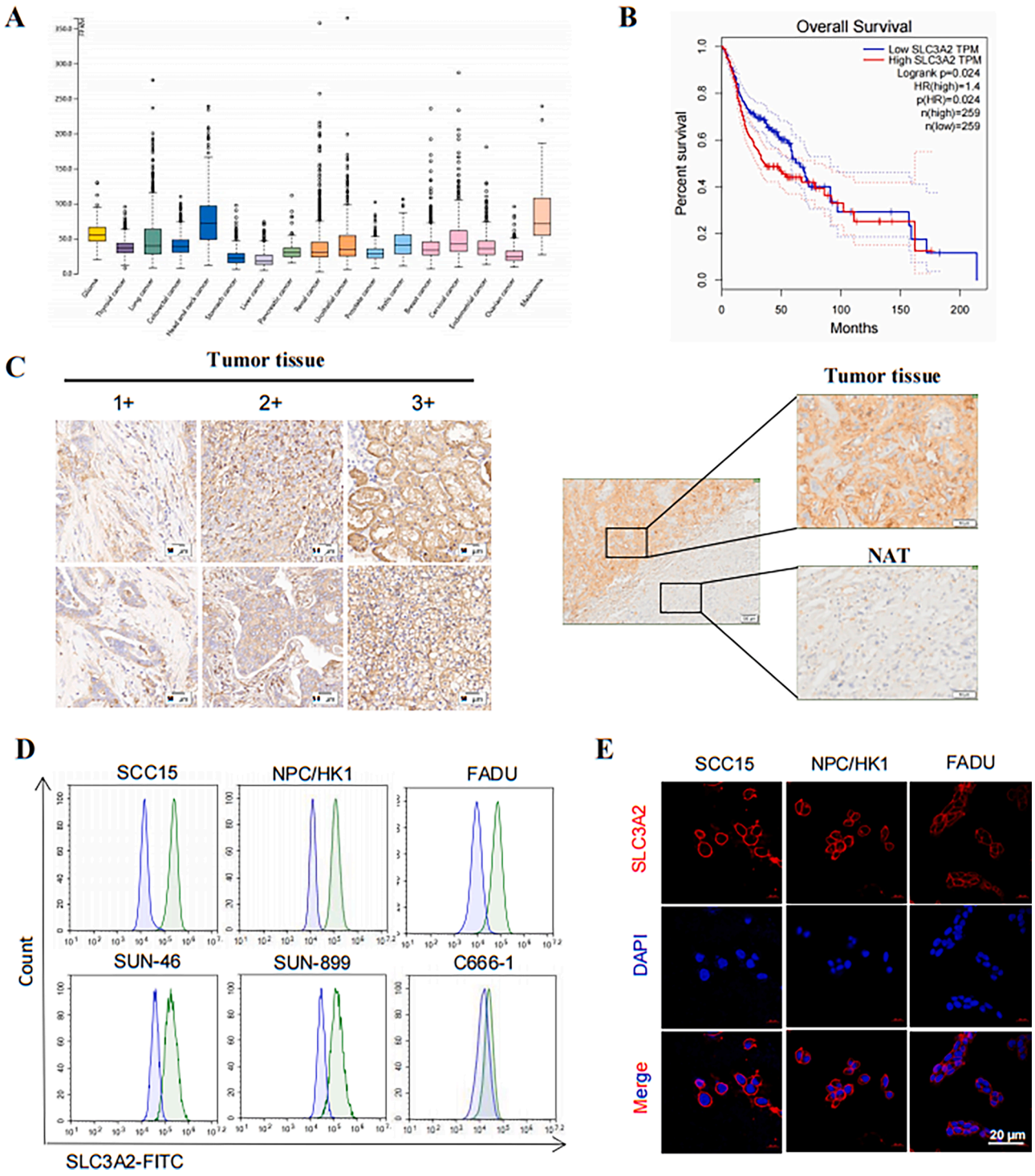


**Fig. 1.** (A) Normalized mRNA levels of SLC3A2 in tumor and normal tissues using the online web server GEPIA. (B) Kaplan-Meier survival curves depicting Overral Survival in HNSCC patients with high and low SLC3A2 expression. (C) Representative images of IHC staining for SLC3A2 expression in HNSCC tissues and normal adjacent tissues (NAT), representing increasing intensity of staining. Scale bars, 50 μm. (D) Flow cytometry analysis of SLC3A2 cell surface expression in a panel of HNSCC cell lines. (E) Immunofluorescence staining with SLC3A2 (red) in three HNSCC cell lines. Cells were incubated with SLC3A2 as the primary antibody and then with the 594-conjugated secondary antibody. Scale bars, 20 μm.

and 6 h. Lysosomal-associated membrane protein 1 (LAMP1) was the lysosome marker for correlating internalized antibodies with lysosomal transport. Following 1-hour incubation, 19G4-MMAE primarily localized to the plasma membrane. However, after 6 h, the cell surface expression of SLC3A2 visibly decreased, with increased co-localization observed with the lysosomal marker LAMP1, indicating the internalization of 19G4-MMAE into NPC/HK1 and SCC15 cells (Fig. 3**A-D**). The interaction with SLC3A2 subsequently facilitated transport to lysosomes, potentially leading to the release of the drug payload into the cytoplasm.

*SLC3A2 mAb induces autophagy in HNSCC*

The expression levels of the protein LC3 are commonly used as an

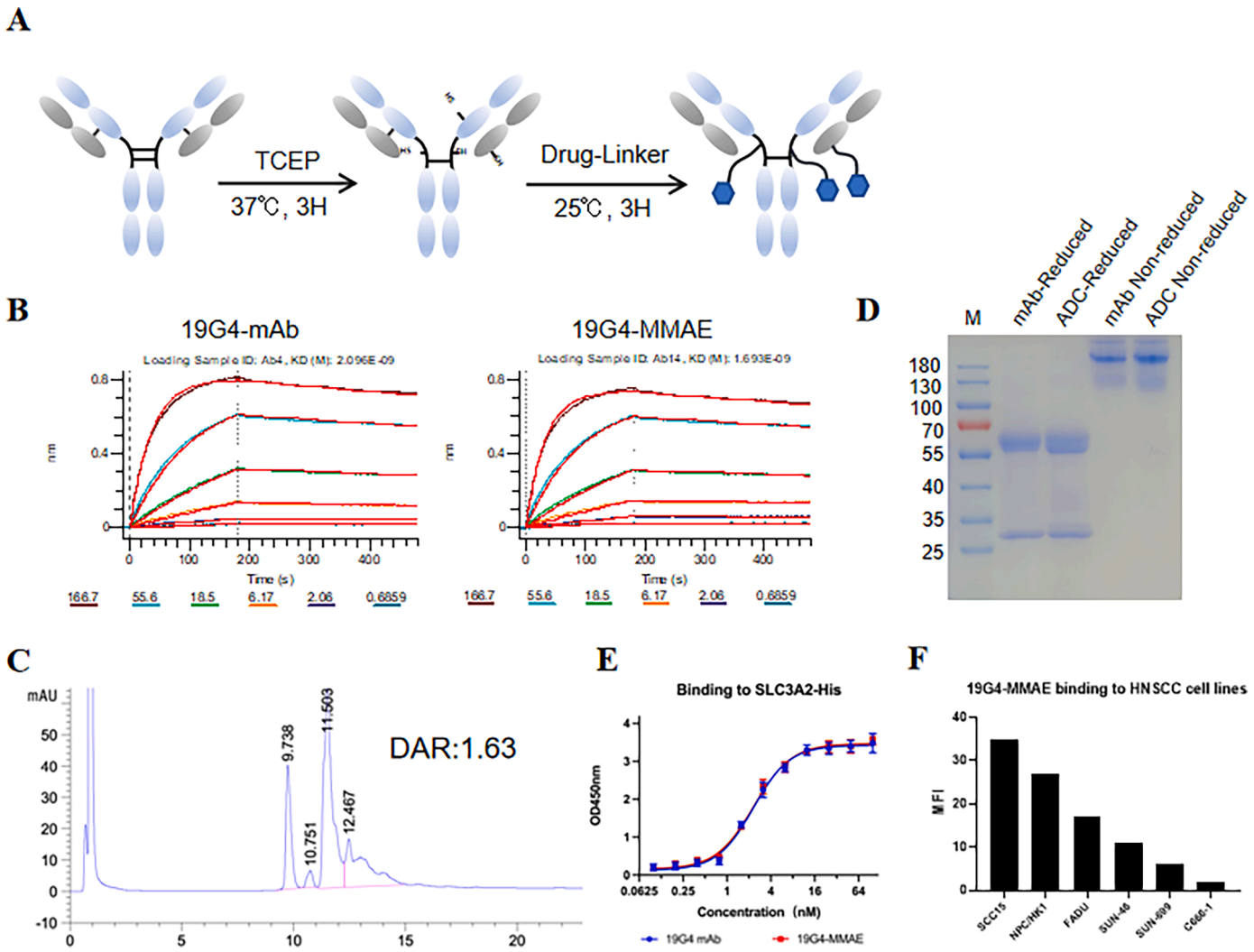


**Fig. 2.** (A) Structure illudion of 19G4-MMAE. (B) The affinity of 19G4 and 19G4-MMAE binding to SLC3A2-ECD-His recombinant protein was determined on an Octet R8 (Sartorius) instrument. (D) Analysis of SDS-PAGE of the antibody-drug conjugates (19G4-MMAE) under non-reducing condition and reducing condition. (E) Binding of 19G4-MMAE to SLC3A2 extracellular domain by ELISA. (F) A panel of HNSCC cells were incubated with 4 μg/mL 19G4-MMAE followed with FITC-labeled goat anti-human IgG (H+L) polyclonal antibody.

autophagosome marker. In this study, immunofluorescence was employed to assess the involvement of autophagy in SLC3A2 targeted therapy to detect the expression of LC3. As shown in Fig. 4**A**, immunofluorescence staining showed significant LC3 expression after 19G4 mAb treatment. Additionally, western blot analysis was conducted to ascertain the expression and conversion of LC3, revealing a marked increase in LC3-II protein levels and a dose-dependent response of SLC3A2 expression in SCC15 cells treated with 19G4 mAb (Fig. 4**B, C**). Furthermore, treatment with the 19G4 mAb decreased the LC3-I/LC3-II ratio, indicating autophagic activation. The elevated levels of LC3-II observed suggest that blocking autophagic degradation may result in LC3-II accumulation [26]. To further investigate the impact of 19G4 mAb on LC3-II levels, the expression of LC3-II was assessed in the presence or absence of chloroquine (CQ, Med Chem Express, Shanghai, China)), a compound that blocks downstream autophagic processes. Interestingly, the addition of CQ resulted in a further increase in LC3-II levels compared to cells exposed to 19G4 alone, confirming the induction of autophagic flux by 19G4 (**Fig. S1A**). These results indicated that SLC3A2-targeted treatment may be associated with intracellular autophagy in SCC15 cells.

*SLC3A2 ADC exhibits specific cytotoxic activity in vitro*

The *in vitro* cytotoxic activity of 19G4-MMAE was investigated using a panel of SLC3A2-positive cell lines (SCC15, NPC/HK1, FADU) and a low SLC3A2-expression cell line, C666-1. These cell lines were treated with 19G4-MMAE, IgG-MMAE, 19G4, or cell medium alone at various concentrations for 72 h. As shown in Fig. 3A, the IC50 values for SLC3A2 ADC in SCC15, NPC/HK1, FADU, and C666-1 cells were 2.02 nM, 205.1 nM, 235.4 nM, and 344.4 μM, respectively. Meanwhile, the isotype control IgG-MMAE and unconjugated antibody 19G4 did not exhibit significant cytotoxic activity. Furthermore, 19G4-MMAE did not show a cell-killing effect on low SLC3A2-expressing C666-1 cells (Fig. 5**A**). The specific antitumor effect of 19G4-MMAE on SCC15 cells at varying concentrations is depicted in Fig. 5**B**, showing inhibition of SCC15 cell growth across the concentration range tested. To assess the impact of autophagy on the cytotoxic activity of 19G4-MMAE, SCC15 cells were co-treated with 19G4-MMAE and the autophagy inhibitor CQ, then we checked cell growth. We found that co-incubation of SCC15 cells with 19G4-MMAE and CQ resulted in comparable cytotoxicity to treatment with either agent alone, indicating that blocking autophagy did not significantly affect the cytotoxic activity of 19G4-MMAE (**Fig. S1B**).

Flow cytometry with annexin V-FITC / 7AAD labeling was utilized to

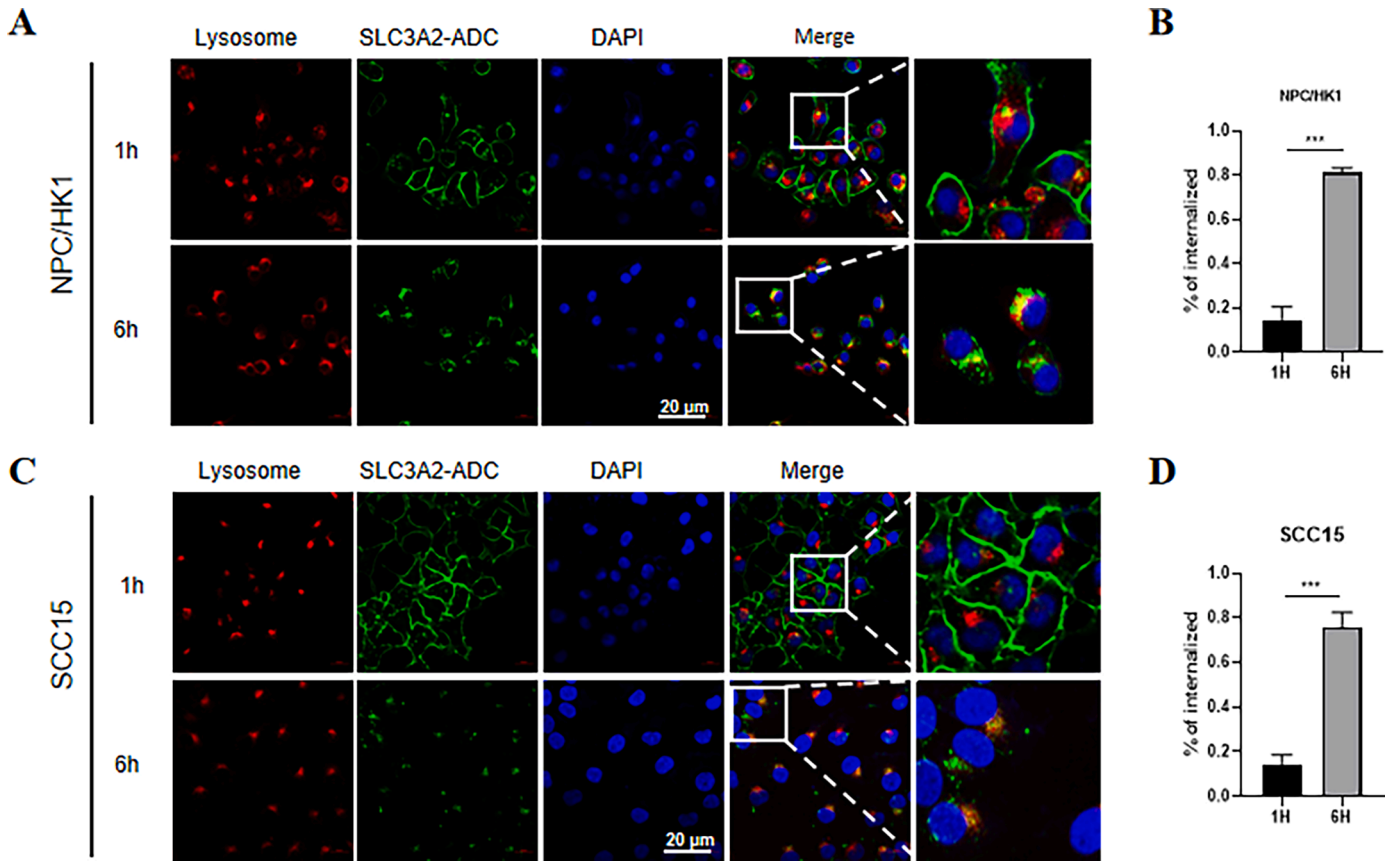


**Fig. 3.** (A,C) SLC3A2-MMAE colocalizes with lysosome in NPC/HK1 and SCC15 cells. NPC/HK1 and SCC15 cells were incubated with 1 hour (upper panel) and 6 h (lower panel) with 19G4-MMAE. Lysosomes were stained with 594-labeled (red) secondary antibody, and SLC3A2 antibodies were stained with FITC-labeled secondary antibody (green), Scale bars, 20 μm. (B,D) Internalization of 19G4-MMAE in NPC/HK1 and SCC15 cells. (For interpretation of the references to color in this figure legend, the reader is referred to the web version of this article.)

calculate the apoptosis induction percentage in the 19G4-MMAE treatment group (Fig. 5**C,** 5**D**). The analysis revealed the proportion of early apoptosis cells (annexin V+/7-AAD−) in SCC15 cells treated with 19G4-MMAE at varying concentrations, showing a concentration-dependent increase in apoptosis induction compared to the control group. To determine whether inhibition of apoptosis could increase the *in vitro* survival of 19G4-MMAE treated cells, SCC15 cells were co-treated with benzyloxycarbonyl-Val-Ala-Asp-fluoromethyl ketone (Z-VAD-FMK, 10 mg/mL) and 19G4-MMAE for 36 h, and we found that co-treated with Z-VAD-FMK significant improves the viability of SCC15 cells, whereas Z-VAD-FMK alone group were not significantly different compare with control group (**Fig. S1C**). Given the significant role of ROS in cancer therapy in triggering apoptosis, we assessed the total ROS levels in SCC15 cells treated with 19G4, IgG-MMAE, and 19G4-MMAE. Treatment with 19G4 notably elevated ROS levels in SCC15 cells (Fig. 5**E**). These findings suggest that the antitumor effects 19G4-MMAE on HNSCC may be attributed to the enhancement of ROS accumulation and the promotion of apoptosis. Due to the SLC3A2 is also involved in ferroptosis [27], to assess the impact of ferroptosis on the cytotoxic activity of the ADC, we co-treated the SCC15 cells with 19G4-MMAE and ferrostatin-1(Med Chem Express, Shanghai, China). However, results in the 19G4-MMAE and ferrostatin-1 co-treated group were not significantly different compared with the 19G4-MMAE alone group. (**Fig. S1D**).

### *In vivo xenograft experiments*

In this study, we investigated the therapeutic efficacy of the 19G4-MMAE conjugate in HNSCC cancer xenografts. The SCC15 cell line was selected to establish mouse subcutaneous tumor models. Mice were administered three doses of PBS, 19G4-MMAE, 19G4, or IgG-MMAE via intravenous injection every three days. The treatment scheme is illustrated in Fig. 6**A**. Consistent with *in vitro* results, the conjugate (5 mg/Kg) significantly reduced tumor burden and significantly increased mouse survival rates (Fig. 6**B,** 6**C**). Treatment with the conjugate (2.5 mg/Kg) resulted in partial tumor growth inhibition, while higher doses (5 or 10 mg/Kg) induced a noticeable delay in tumor progression. In contrast, mice treated with PBS exhibited rapid tumor growth, with no significant inhibition observed in the 19G4 and IgG-MMAE groups (Fig. 6**D**). The effect of the 19G4-MMAE on the mitotic index (Ki67) in SCC15 cells was detected by IHC staining (**Fig. S1E, S1F**). A significant reduction in the Ki67 levels was observed after treatment with 19G4-MMAE. To assess therapy-related nonspecific toxicity, we monitored body weight and organ health throughout the study. As shown in Fig. 6**E**, mice bearing SCC15 tumors did not experience significant weight loss in the 19G4-MMAE treatment group, even at higher concentrations (5 or 10 mg/Kg) (Fig. 6**F**). Moreover, no significant pathological damage was observed in any dose of the 19G4-MMAE group compared to the vehicle group, as evidenced by H&E staining of the organs (Fig. 6**G**).

## Discussion

Novel therapeutic strategies are in high demand for the treatment of HNSCC. ADC targeting tumor-specific surface antigens has demonstrated clinical effectiveness in hematologic and solid malignancies [28]. Our study discovered a significant upregulation of SLC3A2 in both HNSCC tissue and cell lines. Subsequently, we engineered a robust

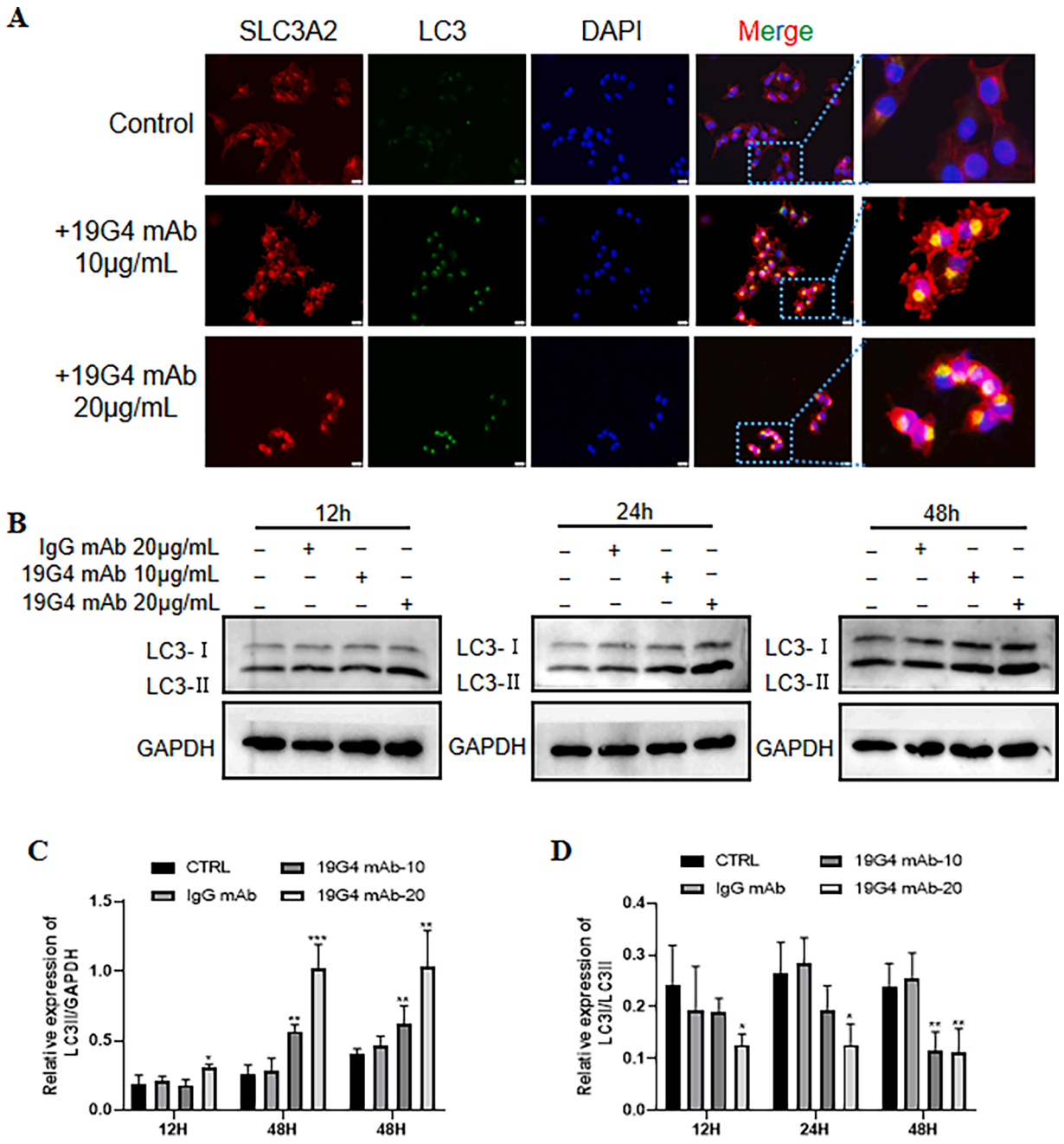


**Fig. 4.** (A) Representative immunofluorescence staining of LC3 in the 19G4 mAb treated group. Scal bar: 20 μm. (B) Representative immunoblotting of LC3 in IgG-mAb, 19G4 mAb (10 μg/mL, 20 μg/mL). (C) Quantification demonstrates that the level of LC3II were significant increase in 19G4 mAb group compared with IgG-mAb group ($p < 0.05$). *** $p < 0.001$,** $p < 0.01$, and * $p < 0.05$ versus the IgG mAb group.

anti-SLC3A2 ADC (19G4-MMAE) that triggered ROS accumulation, stimulated apoptosis in SLC3A2-positive HNSCC cells and demonstrated potent antitumor effects derived from MMAE in preclinical models. These findings propose that targeting SLC3A2 with an anti-SLC3A2 ADC could represent a promising therapeutic avenue for the treatment of HNSCC patients.

The efficacy of the ADC greatly depends on the expression of the target antigen and the antibody internalization. Optimal antitumor activity and minimal toxicity are achieved when the target antigen is predominantly expressed in tumor cells instead of normal cells [8]. Our findings revealed that SLC3A2 exhibited specific expression in HNSCC tissue, while normal tissue displayed little to no SLC3A2 expression. SLC3A2 upregulation was associated with tumor progression across various human cancer types, such as melanoma, lung adenocarcinoma, colorectal cancer, breast cancer, renal cell carcinoma, and hepatocellular carcinoma [29]. Additionally, Sun et al. demonstrated that elevated SLC3A2 levels on cell membranes promoted proliferation in oral squamous cancer cells, whereas SLC3A2 knockdown inhibited tumor cell migration and invasion [30]. Consistent with prior studies, our research identified high SLC3A2 expression in HNSCC, with elevated levels correlating with poorer prognoses. These characteristics position SLC3A2 as a promising target for targeted and combination therapy in HNSCC.

Efficient antibody-mediated internalization and lysosomal targeting are crucial for ensuring the efficacy of ADCs. Milkereit et al. demonstrated that LAPTM4b can recruit LAT1-CD98hc to the lysosome [23], suggesting that SLC3A2 plays a pivotal role in the efficient internalization and delivery of the potent payload to the cytosol, thus making it a

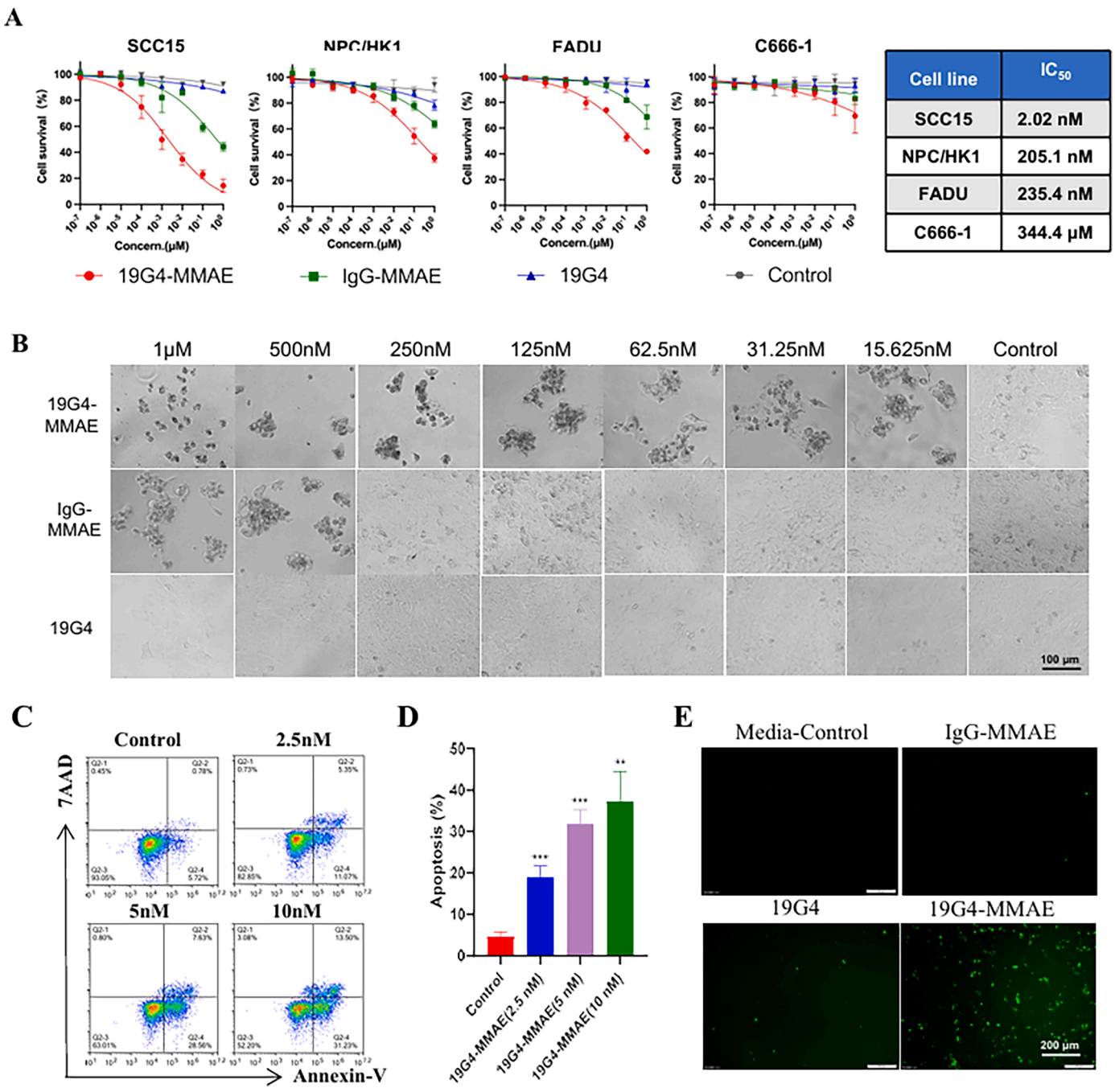


| Cell line | $IC_{50}$ |
|---|---|
| SCC15 | 2.02 nM |
| NPC/HK1 | 205.1 nM |
| FADU | 235.4 nM |
| C666-1 | 344.4 μM |

**Fig. 5.** (A) *In vitro* efficacy of 19G4-MMAE versus 19G4, IgG-MMAE and control (cell medium) on four HNSCC cell lines treated for 72 h, including SCC15,NPC/HK1, FADU, and C666–1. The IC50 values are shown in the box. (B) Effect of 19G4-MMAE with different concentrations (72 h) on the SCC15 cells. Scale bars, 100 μm. (C) SCC15 cells were exposed to medium, 19G4-MMAE at indicated concentrations for 48 h, cell apoptosis was assessed by flow cytometry. (D) The percentage of apoptosis cells are depicted in bar charts. (E) ROS accumulation was determined in SCC15 cells after treatment with medium control, 19G4, IgG-MMAE, and 19G4-MMAE for 24 h. Representative immunoflaurence images of ROS staining with the green fluorescence signal confirm intracellular ROS accumulation. (For interpretation of the references to color in this figure legend, the reader is referred to the web version of this article.)

promising candidate for ADC development. In our investigation, the binding of antibodies to the extracellular domain of human SLC3A2 enabled us to investigate the internalization characteristics of 19G4-MMAE in HNSCC cell lines. Notably, the colocalization of SLC3A2 expression with the lysosomal marker LAMP1 confirmed the ability of SLC3A2 to be directed to lysosomes, where 19G4-MMAE is processed intracellularly [31], underscoring its potential as a crucial mediator of lysosomal delivery and internalization. Furthermore, Parren et al. developed a bispecific antibody-drug conjugate (bsADC) targeting a lysosomal-delivered protein, demonstrating enhanced intracellular delivery of ADCs [32]. Zhuang et al. engineered a novel bsADC targeting HER2 and Sortilin-1 (SORT1) with robust internalization activity and cytotoxicity against HER2-low-expression tumor cells [33]. Thus, SLC3A2 could serve as a viable target for constructing bispecific ADCs to enhance lysosomal targeting and internalization, potentially even with tumor-specific antigens with poor internalization characteristics.

Besides, the SLC7A5/SLC3A2 is a heterodimeric bidirectional amino acid transport that regulates the exchange of intracellular l-glutamine for extracellular l-leucine. Niklin et al. found that the reciprocal transport of l-glutamine and essential amino acids (EAAs) regulates mTORC1

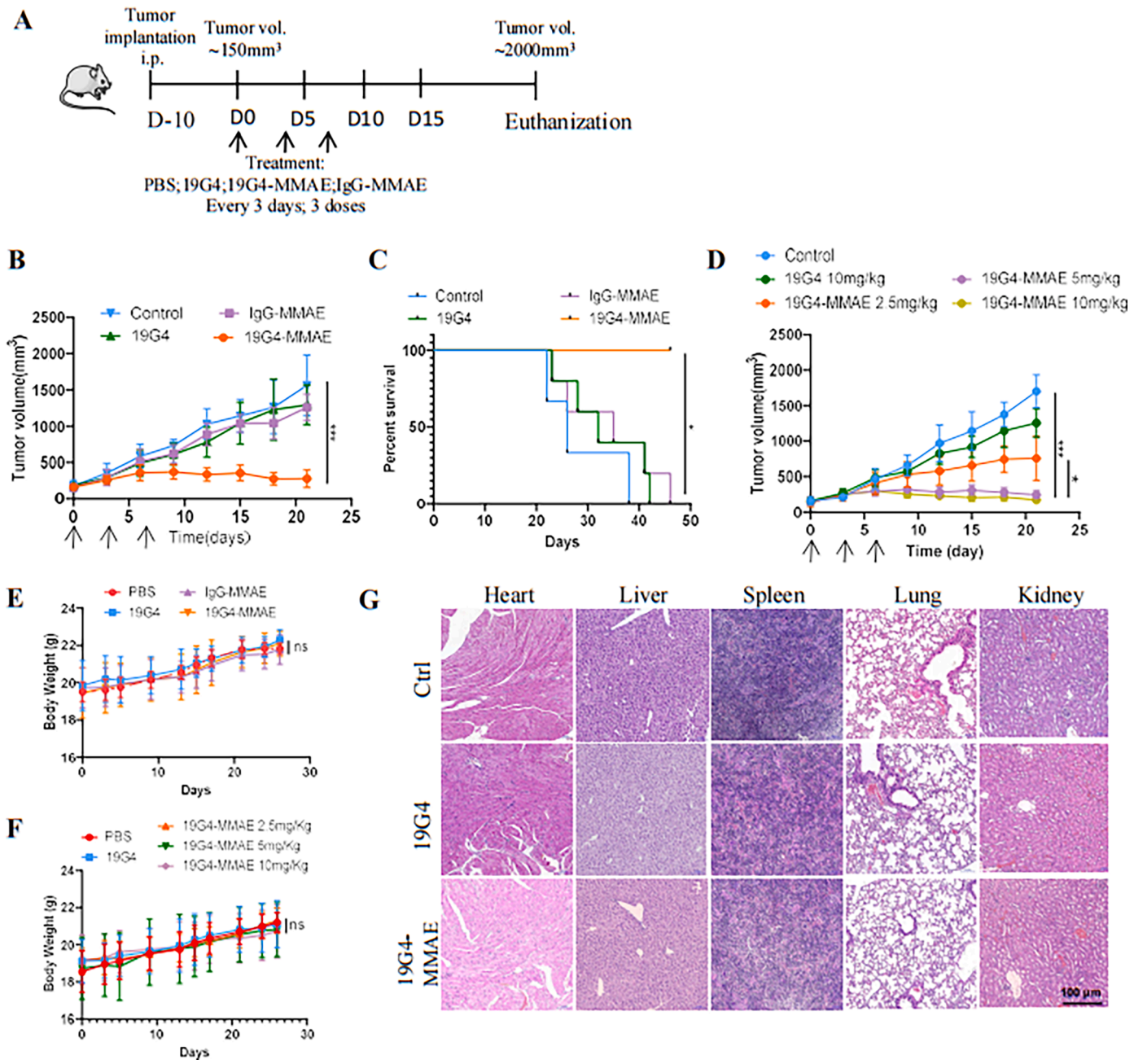


**Fig. 6.** (A) The treatment scheme of SCC15 BALB/c nude mouse models. (B) SCC15 cells were subcutaneously injected into right flanks of BALB/c nude mice, animal were randomly assigned to vehicle PBS, 19G4, IgG-MMAE and 19G4-MMAE(5 mg/kg), Mice were monitored for tumor growth, tumor masses were measured using a digital caliper. (C) PFS for the different treatment groups shown in B. (D) SCC15 cells were subcutaneously injected into right flanks of BALB/c nude mice, animal were randomly assigned to vehicle PBS, 19G4-MMAE 2.5 mg/kg, 19G4-MMAE 5 mg/kg or 19G4-MMAE 10 mg/kg. Mice were monitored for tumor growth, tumor masses were measured using a digital caliper. (E) Bodyweight changes of Balb/c nude mice after the treatment of PBS (control), 19G4, IgG-MMAE, 19G4-MMAE, Error bars represent standard error of the mean. (F) Bodyweight changes of Balb/c nude mice after the treatment of 19G4 or 19G4-MMAE at 2.5, 5, 10 mg/Kg. (G) H&E staining of vital organ of BALB/c nude mice after treatment with PBS (control), 19G4, 19G4-MMAE for a total of three doses. Magnification: × 100. Black scale bar: 100 μm.

signaling and autophagy [34]. Consistently, Digomann et al. demonstrated that reducing SLC3A2 expression inhibits the mTOR pathway and triggers autophagy [35]. Thus, this study investigated whether targeting SLC3A2 could induce autophagy. Specifically, we assessed the levels of LC3, a widely used autophagosome marker. Our findings showed that treatment with the 19G4 monoclonal antibody induces autophagy, as confirmed by immunofluorescence staining. Quantitative western blotting revealed that 19G4 treatment enhances autophagic activity by increasing LC3 expression. The conversion of LC3-I to LC3-II proteins is a well-known indicator of autophagy. Following 19G4 treatment, we observed a decrease in the LC3-I/LC3-II ratio, indicative of autophagy induction. Interestingly, blocking autophagy with chloroquine did not significantly impact the cytotoxic effects of 19G4-MMAE. Additionally, treatment with the nude anti-SLC3A2 antibody did not notably affect the proliferation of the HNSCC cell line tested. The role of autophagy in SLC3A2-targeted therapy warrants further investigation. Although, autophagy inhibition did not significant relieve the 19G4-MMAE induced growth inhibition of HNSCC cells. Targeting SLC3A2 may trigger autophagy and therefore enhance cellular radiosensitivity as a cellular stress response mechanism [17,34]. The

expression of SLC3A2 in HNSCC cells plays a crucial role in regulating tumor radiosensitivity. Integrating SLC3A2-targeted therapy with radiotherapy may be a promise for translational research in clinical settings.

We investigated the potential efficacy of 19G4-MMAE in treating HNSCC. To evaluate its effectiveness, we examined the antitumor activity of 19G4-MMAE in various HNSCC cell lines. Our findings demonstrated that 19G4-MMAE exhibited a strong anti-proliferative effect in SLC3A2-positive cell lines tested, contrasting with the lack of significant antitumor activity of the nude anti-SLC3A2 (19G4) antibody *in vitro*, indicating that the cytotoxic drug linked to the nude antibody is responsible for the observed anti-proliferative effects. Conversely, SLC3A2-negative HNSCC cells showed little response to 19G4-MMAE treatment. Notably, SLC7A5 and SLC3A2 play essential roles in tumor growth and the regulation of oxidative stress through amino acid transport mechanisms [30]. Furthermore, we measured the total level of ROS in SCC15 cells and observed a substantial increase in ROS accumulation in SCC15 cells treated with 19G4-MMAE compared to those treated with 19G4 or IgG-MMAE. Additionally, 19G4-MMAE treatment induced apoptosis in an oxidative stress-dependent manner. Importantly, Z-VAD-FMK treatment improve the viability of 19G4-MMAE treated SCC 15 cells. In this study, we also explore the impact of ferroptosis on cytotoxic activity of the ADC. However, results in the 19G4-MMAE and ferrostatin-1 co-treated group were not significant different compared with the ADC group. The inefficiency of ferrostatin-1 to prevent 19G4-MMAE induced cell death in the present study may be due to the fact that SLC3A2 mAb does not inhibit all l-glutamine intake to the same extent. Taken together, it is speculated that 19G4-MMAE treatment leads to heightened ROS levels and triggers apoptosis in SLC3A2-positive HNSCC cells.

In assessing the antitumor effects 19G4-MMAE in SLC3A2-positive cell line-derived mouse models, 19G4-MMAE demonstrated a strong selective antitumor efficacy against the SLC3A2-positive mouse models examined in our study. Safety is a critical aspect of evaluating an ADC. Therefore, safety assessments were carried out in BALB/c nude mice, revealing no signs of toxicity in the group receiving 19G4-MMAE. Our results indicated that 19G4-MMAE was well-tolerated at therapeutic dosages in BALB/c nude mice. Notably, severe cachexia was not observed in the group treated with 19G4-MMAE compared to the control group. The relationship between systemic changes affecting tumor growth and the development of milder cachexia is likely to be variable and, therefore, remains a topic of debate. The association between tumor burden and cachexia is not fully understood and requires further investigation [36,37].

This study has certain limitations. The anti-SLC3A2 antibodies employed in the ADC generation target human SLC3A2 and do not recognize the mouse counterpart. Therefore, interpretations regarding the absence of toxicity should be approached with caution. Conducting studies with immune-competent HNSCC mouse models treated with a SLC3A2-targeted ADC that recognizes the murine protein may assist in more accurately assessing drug-related toxicity and efficacy.

Our results revealed that anti-SLC3A2 ADC (19G4-MMAE) effectively suppressed the proliferation of SLC3A2-positive HNSCC cells, inhibited the growth of SLC3A2-positive HNSCC xenograft models, and demonstrated favorable safety profiles in animal studies. The identification of SLC3A2 internalization and lysosomal targeting properties, combined with the anticancer efficacy of the ADC against SLC3A2, suggest that anti-SLC3A2 ADC holds promise as a therapeutic candidate for ADC therapy in treating HNSCC patients.

## Funding

This work was jointly sponsored by Post-Doctor Research Project, West China Hospital, Sichuan University (No.2023HXBH099), Science and Technology Department of Sichuan Province, PR China (No. 2022NSFSC0847 & 2022NSFSC0851).

## Consent for publication

All authors give consent for publication.

## CRediT authorship contribution statement

**Meijun Zheng:** Writing – original draft, Methodology, Funding acquisition. **Zeng Wang:** Writing – original draft, Validation, Methodology. **Mengyao Li:** Writing – review & editing, Validation. **Nian Yang:** Writing – review & editing, Validation, Methodology. **Huaqing Lu:** Writing – review & editing, Methodology. **Zongliang Zhang:** Writing – review & editing, Validation, Methodology. **Yijun Dong:** Writing – review & editing, Validation. **Yongdong Chen:** Writing – review & editing, Validation. **Zhixiong Zhu:** Writing – review & editing. **Aiping Tong:** Writing – review & editing, Supervision, Project administration, Conceptualization. **Hui Yang:** Writing – review & editing, Supervision, Funding acquisition, Conceptualization.

## Declaration of competing interest

The authors declare no competing interests.

## Data availability

The data that support the findings of this study are available from the corresponding author upon reasonable request.

## Supplementary materials

Supplementary material associated with this article can be found, in the online version, at doi:10.1016/j.tranon.2024.101981.

## References

[1] F. Bray, J. Ferlay, I. Soerjomataram, R.L. Siegel, L.A. Torre, A. Jemal, Global cancer statistics 2018: GLOBOCAN estimates of incidence and mortality worldwide for 36 cancers in 185 countries, CA Cancer J. Clin. 68 (6) (2018) 394–424, https://doi.org/10.3322/caac.21492.

[2] R. Mandal, Y. Senbabaoglu, A. Desrichard, J.J. Havel, M.G. Dalin, N. Riaz, K. W. Lee, I. Ganly, A.A. Hakimi, T.A. Chan, L.G. Morris, The head and neck cancer immune landscape and its immunotherapeutic implications, JCI Insight 1 (17) (2016) e89829, https://doi.org/10.1172/jci.insight.89829.

[3] M.L. Gillison, A.K. Chaturvedi, W.F. Anderson, C. Fakhry, Epidemiology of human papillomavirus-positive head and neck squamous cell carcinoma, J. Clin. Oncol. 33 (29) (2015) 3235–3242, https://doi.org/10.1200/JCO.2015.61.6995.

[4] A. Wyss, M. Hashibe, S.C. Chuang, Y.C. Lee, Z.F. Zhang, et al., Cigarette, cigar, and pipe smoking and the risk of head and neck cancers: pooled analysis in the International Head and Neck Cancer Epidemiology Consortium, Am. J. Epidemiol. 178 (5) (2013) 679–690, https://doi.org/10.1093/aje/kwt029.

[5] F. De Felice, V. Tombolini, M. de Vincentiis, G. Magliulo, A. Greco, V. Valentini, A. Polimeni, Multidisciplinary team in head and neck cancer: a management model, Med. Oncol. 36 (1) (2018) 2, https://doi.org/10.1007/s12032-018-1227-z. PMID: 30426243.

[6] J.P. Machiels, C. René Leemans, W. Golusinski, et al., Squamous cell carcinoma of the oral cavity, larynx, oropharynx and hypopharynx: EHNS-ESMO-ESTRO Clinical Practice Guidelines for diagnosis, treatment and follow-up, Ann. Oncol. 31 (11) (2020) 1462–1475, https://doi.org/10.1016/j.annonc.2020.07.011.

[7] T.L. Whiteside, Head and neck carcinoma immunotherapy: facts and hopes, Clin. Cancer Res. 24 (1) (2018) 6–13, https://doi.org/10.1158/1078-0432.

[8] A.S. Köseer, L.R. Loureiro, J. Jureczek, N. Mitwasi, S. González, et al., Validation of CD98hc as a therapeutic target for a combination of radiation and immunotherapies in head and neck squamous cell carcinoma, Cancers 14 (7) (2022), https://doi.org/10.3390/cancers14071677.

[9] U. Hafeez, S. Parakh, H.K. Gan, A.M. Scott, Antibody–drug conjugates for cancer therapy, Molecules 25 (20) (2020), https://doi.org/10.3390/molecules25204764.

[10] H.L. Perez, P.M. Cardarelli, S. Deshpande, S. Gangwar, G.M. Schroeder, et al., Antibody–drug conjugates: current status and future directions, Drug Discov. Today 19 (7) (2014) 869–881, https://doi.org/10.1016/j.drudis.2013.11.004.

[11] E. Komlodi-Pasztor, D.L. Sackett, A.T. Fojo, Inhibitors targeting mitosis: tales of how great drugs against a promising target were brought down by a flawed rationale, Clin. Cancer Res. 18 (1) (2012) 51–63, https://doi.org/10.1158/1078-0432.CCR-11-0999.

[12] K. Carlson, A.J. Ocean, Peripheral neuropathy with microtubule-targeting agents: occurrence and management approach, Clin. Breast. Cancer 11 (2) (2011) 73–81, https://doi.org/10.1016/j.clbc.2011.03.006.
[13] D.M. Roque, S. Bellone, D.P. English, N. Buza, E. Cocco, et al., Tubulin-β-III overexpression by uterine serous carcinomas is a marker for poor overall survival after platinum/taxane chemotherapy and sensitivity to epothilones, Cancer 119 (14) (2013) 2582–2592, https://doi.org/10.1002/cncr.28017.
[14] L. Lin, S.W. Yee, R.B. Kim, K.M. Giacomini, SLC transporters as therapeutic targets: emerging opportunities, Nat. Rev. Drug Discov. 14 (8) (2015) 543–560, https://doi.org/10.1038/nrd4626.
[15] K. Hasegawa, S. Ikeda, M. Yaga, K. Watanabe, R. Urakawa, et al., Selective targeting of multiple myeloma cells with a monoclonal antibody recognizing the ubiquitous protein CD98 heavy chain, Sci. Transl. Med. 14 (632) (2022) eaax7706, https://doi.org/10.1126/scitranslmed.aax7706.
[16] M. Poettler, M. Unseld, K. Braemswig, A. Haitel, C.C. Zielinski, G.W. Prager, CD98hc (SLC3A2) drives integrin-dependent renal cancer cell behavior, Mol. Cancer 12 (2013) 169, https://doi.org/10.1186/1476-4598-12-169.
[17] Z. Li, S. Chen, X. He, S. Gong, L. Sun, L. Weng, SLC3A2 promotes tumor-associated macrophage polarization through metabolic reprogramming in lung cancer, Cancer Sci. 114 (6) (2023) 2306–2317, https://doi.org/10.1111/cas.15760.
[18] J.C. Montero, E. Calvo-Jiménez, S. del Carmen, M. Abad, A. Ocaña, A. Pandiella, Surfaceome analyses uncover CD98hc as an antibody drug-conjugate target in triple negative breast cancer, J. Exp. Clin. Cancer Res. 41 (1) (2022), https://doi.org/10.1186/s13046-022-02330-4.
[19] D. Digomann, I. Kurth, A. Tyutyunnykova, O. Chen, S. Löck, et al., The CD98 heavy chain is a marker and regulator of head and neck squamous cell carcinoma radiosensitivity, Clin. Cancer Res. 25 (10) (2019) 3152–3163, https://doi.org/10.1158/1078-0432.CCR-18-2951.
[20] D.M. Salter, A.S. Krajewski, T. Sheehan, G. Turner, R.J. Cuthbert, A. Mclean, Prognostic significance of activation and differentiation antigen expression in B-cell non-Hodgkin's lymphoma, J. Pathol. 159 (3) (1989) 211–220, https://doi.org/10.1002/path.1711590307.
[21] J. Bajaj, T. Konuma, N.K. Lytle, Hyog Y. Kwon, J.N.; Ablack, et al., CD98-mediated adhesive signaling enables the establishment and propagation of acute myelogenous leukemia, Cancer Cell 30 (5) (2016) 792–805, https://doi.org/10.1016/j.ccell.2016.10.003.
[22] M. Toyoda, K. Kaira, M. Shino, K. Sakakura, K. Takahashi, et al., CD98 as a novel prognostic indicator for patients with stage III/IV hypopharyngeal squamous cell carcinoma, Head Neck 37 (11) (2015) 1569–1574, https://doi.org/10.1002/hed.23797.
[23] R. Milkereit, A. Persaud, L. Vanoaica, A. Guetg, F. Verrey, D. Rotin, LAPTM4b recruits the LAT1-4F2hc Leu transporter to lysosomes and promotes mTORC1 activation, Nat. Commun. 6 (2015) 7250, https://doi.org/10.1038/ncomms8250.
[24] H. Tu, L.J. Tang, X.J. Luo, K.L. Ai, J. Peng, Insights into the novel function of system Xc- in regulated cell death, Eur. Rev. Med. Pharmacol. Sci. 25 (3) (2021) 1650–1662, https://doi.org/10.26355/eurrev_202102_24876.
[25] D. Criscuolo, F. Morra, A. Celetti, A xCT role in tumour-associated ferroptosis shed light on novel therapeutic options, Explor. Target. Antitumor. Ther. 3 (5) (2022) 570–581, https://doi.org/10.37349/etat.2022.00101.
[26] N. Mizushima, Autophagy: process and function, Genes Dev. 21 (22) (2007) 2861–2873, https://doi.org/10.1101/gad.1599207.
[27] F. Wu, G. Xiong, Z. Chen, C. Lei, Q. Liu, Y. Bai, SLC3A2 inhibits ferroptosis in laryngeal carcinoma via mTOR pathway, Hereditas 159 (1) (2022) 6, https://doi.org/10.1186/s41065-022-00225-0.
[28] R.M. DeVay, K. Delaria, G. Zhu, C. Holz, D. Foletti, et al., Improved lysosomal trafficking can modulate the potency of antibody drug conjugates, Bioconjug. Chem. 28 (4) (2017) 1102–1114, https://doi.org/10.1021/acs.bioconjchem.7b00013.
[29] G. Pellizzari, O. Martinez, S. Crescioli, R. Page, A. Di Meo, et al., Immunotherapy using IgE or CAR T cells for cancers expressing the tumor antigen SLC3A2, J. ImmunOther Cancer 9 (6) (2021), https://doi.org/10.1136/jitc-2020-002140.
[30] J. Liang, Z. Sun, Overexpression of membranal SLC3A2 regulates the proliferation of oral squamous cancer cells and affects the prognosis of oral cancer patients, J. Oral Pathol. Med. 50 (4) (2021) 371–377, https://doi.org/10.1111/jop.13132.
[31] H.K. Erickson, P.U. Park, W.C. Widdison, Y.V. Kovtun, L.M. Garrett, et al., Antibody-maytansinoid conjugates are activated in targeted cancer cells by lysosomal degradation and linker-dependent intracellular processing, Cancer Res. 66 (8) (2006) 4426–4433, https://doi.org/10.1158/0008-5472.CAN-05-4489.
[32] B.E.C.G. De Goeij, T. Vink, H. ten Napel, E.C.W. Breij, D. Satijn, R. Wubbolts, D. Miao, P.W.H.I. Parren, Efficient payload delivery by a bispecific antibody–drug conjugate targeting HER2 and CD63, Mol. Cancer Ther. 15 (11) (2016) 2688–2697, https://doi.org/10.1158/1535-7163.MCT-16-0364.
[33] W. Zhuang, W. Zhang, L. Wang, L. Xie, J. Feng, B. Zhang, Y. Hu, Generation of a novel SORT1×HER2 bispecific antibody-drug conjugate targeting HER2-low-expression tumor, Int. J. Mol. Sci. 24 (22) (2023) 16056, https://doi.org/10.3390/ijms242216056.
[34] D. Digomann, A. Linge, A. Dubrovska, SLC3A2/CD98hc, autophagy and tumor radioresistance: a link confirmed, Autophagy. 15 (10) (2019) 1850–1851, https://doi.org/10.1080/15548627.2019.1639302.
[35] P. Nicklin, P. Bergman, B. Zhang, E. Triantafellow, H. Wang, B. Nyfeler, H. Yang, M. Hild, C. Kung, C. Wilson, V.E. Myer, J.P. MacKeigan, J.A. Porter, Y.K. Wang, L. C. Cantley, P.M. Finan, L.O. Murphy, Bidirectional transport of amino acids regulates mTOR and autophagy, Cell 136 (3) (2009) 521–534, https://doi.org/10.1016/j.cell.2008.11.044.
[36] A. De Lerma Barbaro, The complex liaison between cachexia and tumor burden (Review), Oncol. Rep. 34 (2015) 1635–1649, https://doi.org/10.3892/or.2015.4164.
[37] A. De Lerma Barbaro, The complex liaison between cachexia and tumor burden (Review), Oncol. Rep. 34 (4) (2015) 1635–1649, https://doi.org/10.3892/or.2015.4164.